THE JOURNAL OF PHYSICAL CHEMISTRY Letters

Letter

pubs.acs.org/JPCL

Spatially Distributed Rheological Properties in Confined Polymers by Noncontact Shear

Mithun Chowdhury,[†,⊥] Yunlong Guo,[†,§,⊥] Yucheng Wang,[†] Weston L. Merling,[∥] Jayachandra H. Mangalara,[∥] David S. Simmons,[*,∥] and Rodney D. Priestley[*,†,‡]

[†]Department of Chemical and Biological Engineering and [‡]Princeton Institute for the Science and Technology of Materials, Princeton University, Princeton, New Jersey 08544, United States

[§]University of Michigan − Shanghai Jiao Tong University Joint Institute, Shanghai Jiao Tong University, Shanghai 200240, P. R. China

[∥]Department of Polymer Engineering, University of Akron, Akron, Ohio 44325, United States

Supporting Information

ABSTRACT: When geometrically confined to the nanometer length scale, a condition in which a large portion of the material is in the nanoscale vicinity of interfaces, polymers can show astonishing changes in physical properties. In this investigation, we employ a unique noncontact capillary nanoshearing method to directly probe nanoresolved gradients in the rheological response of ultrathin polymer films as a function of temperature and stress. Results show that ultrathin polymer films, in response to an applied shear stress, exhibit a gradient in molecular mobility and viscosity that originates at the interfaces. We demonstrate, via molecular dynamics simulations, that these gradients in molecular mobility reflect gradients in the average segmental relaxation time and the glass-transition temperature.

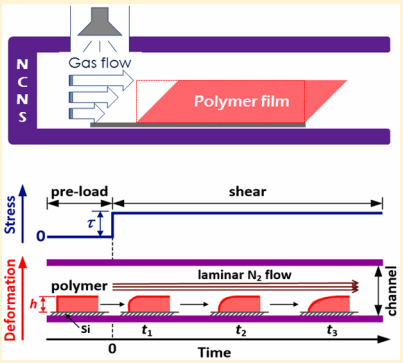

The confinement of polymeric materials to the nanoscale has enabled the development of new materials[1−3] and functional devices[4,5] that impact a myriad of emerging technologies[2−4] and challenge our fundamental understanding of materials' behavior.[6−14] In geometrically confined polymers, as the confining dimension (e.g., thickness for thin films[12,13,15−17] or interparticle spacing for nanocomposites[8,14,18]) is reduced, an increasingly large portion of the polymeric material is in close proximity to an interface.[6] The presence of supporting interfaces can affect the molecular mobility of polymers through the formation of nonequilibrium states,[19−21] for instance, the formation of an irreversibly adsorbed polymer layer.[6,22] In these confined states, in which interfacial effects can perturb mean structure and dynamics,[6,9,16,17,19,21,23] astonishing changes in material properties have been reported, including in the glass-transition temperature (T_g),[6,9,13,15,16,22,24−28] fracture toughness,[10] viscosity,[12,13,20,29−33] modulus,[11,12,34,35] and compliance.[36] It has been shown that these interfacial effects can reflect a spatial gradient in T_g that correlates well with its size-dependent changes.[15,17] A broader perspective on the origin of gradients in molecular mobility of confined polymers has been very recently addressed.[6] However, it remains unclear whether shifts in T_g, diffusion, and viscosity are correlated in nanoconfined polymers.[13] While several experiments have been designed to measure the viscoelastic properties of confined polymers,[12,19,21,33,35−37] they have generally directly measured only average properties, with spatial distributions indirectly inferred based on layer-model interpretations of average mechanical responses.[13,30] While several techniques are capable of directly measuring viscoelastic properties at the free surface of confined polymers,[12,37,38] direct depth-resolved analysis still remains a challenge. Direct access to spatially resolved rheological properties in confined polymers would provide fundamental insights into how interfaces and finite-size effects combine to modify viscoelastic functions,[23,25,27] allow for the identification of correlations between spatially distributed properties,[15,17] and aid in the development of novel processing routes to generate nanostructured polymers.[2]

It has been recognized for over a decade that there is an important "need to understand how the mechanical properties of matter are changed by the proximity of interfaces".[16] To enable a direct experimental probe of this issue, we introduce a noncontact capillary nanoshearing (NCNS) method that allows for the measurement of spatially resolved time-dependent viscoelastic functions of ultrathin polymer films supported atop a substrate. We focus our study on low-molecular-weight (M_w = 2.5 kDa) polystyrene (PS) because its average viscosity has been characterized in the thin-film geometry.[30,31,33] We show that NCNS reports the depth-resolved thermoviscoelastic

Received: January 27, 2017
Accepted: February 21, 2017
Published: March 3, 2017

DOI: 10.1021/acs.jpclett.7b00214
J. Phys. Chem. Lett. 2017, 8, 1229−1234

properties of a polystyrene thin film on a solid substrate by applying a controlled air shear stress and measuring the resulting time-dependent strain gradient while controlling the temperature of the system. We find that shear mobility increases from the bulk to the free surface, reflecting a reduction in viscosity upon approach to the surface of the film. The physical origin of this finding in terms of local alterations in segmental dynamics is further elucidated via molecular dynamics simulation of NCNS performed on a model bead−spring polymer. Further experiments on temperature variation of effective average film viscosity compare well with literature values for thin films.

The NCNS method is a noncontact approach to measure polymer deformation under shear induced by gas flow, inspired by the blow-off method first introduced by Derjaguin[39] and later applied by others.[40,41] In the experiment, a thin liquid film supported atop a solid substrate is placed inside a microchannel, as shown in Figure 1. The dimensions of the channel

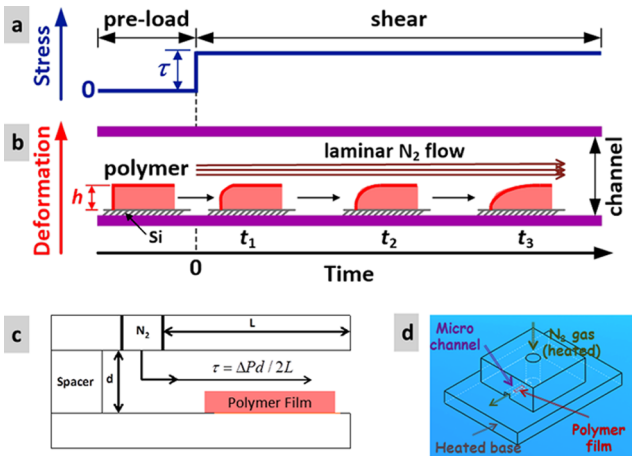

Figure 1. Schematic of NCNS protocol showing (a) constant shear stress on the polymer film and (b) polymer film deformation under stress induced by laminar gas flow in a microchannel. Schematic drawings (c) of the NCNS flow cell consisting of a microchannel with gas in/out-lets and (d) assembly of the NCNS system.

are designed to enable laminar gas flow inside the cell.[40,41] Consequently, the gas flow results in an applied shear stress on the film.[40] In response to the applied shear stress, the time-dependent deformation of the film can be observed by monitoring the evolution of the film profile. Spatially resolved viscoelastic functions can then be computed in a layer-by-layer approach. Figure 1a,b show the schematic of the experimental protocol.

We designed and fabricated a flow cell apparatus in which nitrogen was used as the gas source (Figure 1c,d). In our design, both the gas source and flow cell are equipped with independent heating systems for temperature control up to 150 °C. The flow cell is designed to achieve a pressure drop (ΔP) corresponding to a shear stress range of 40 to 175 Pa. From the well-known Hagen−Poiseuille relationship the shear stress within the flow cell can be calculated as[40,41] $\tau = \Delta Pd/2L$, where d and L are geometric parameters of the cell (Figure 1c).

For NCNS experiments, spin-coated PS (M_w = 2.5 kDa) films (thickness ∼110 nm) were subjected to a mechanical cleavage,[31] leading to a sharp step-edge. It is important in the NCNS experiment that any change in shape of the step-edge is due to the shear stress imposed by the gas flow. To examine this constraint we did a set of control experiments involving thermal annealing of nominally similar films on top of different wettable substrates. It enabled us to disentangle the role of NCNS, capillary leveling,[29,33] and dewetting[31] (see the Supporting Information, Figure S1a−d).

Figure 2a displays the step-edge profile (shifted to step-edge origin) for a 110 nm thick film subjected to an applied shear

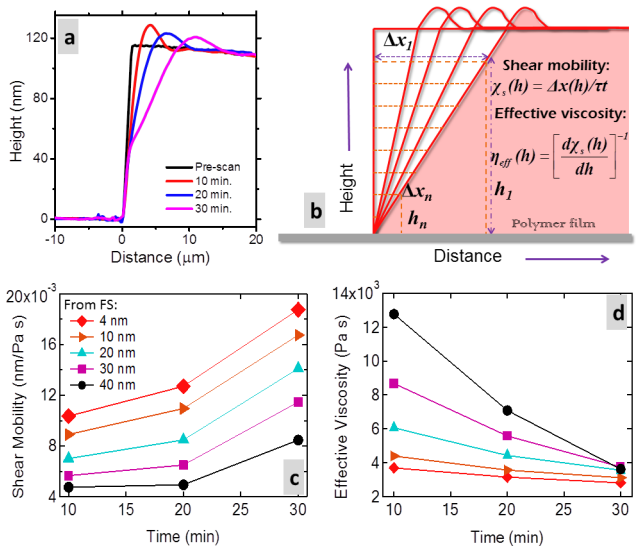

Figure 2. NCNS of PS 2.5 kDa, ∼110 nm film thickness at 108.5 °C (T_g + 52 °C). Applied shear stress during NCNS = 174 Pa. (a) Tapping mode AFM height profiles with time of shear. Rim formation is due to instability on the nonwettable substrate. Gradual tilting of step-edge profile with time shows the effect of the shear stress. Region above ∼40 nm of film thickness exhibiting notable effect of shear as shown by tilted profiles (shifted and superposed to the step-edge origin). (b) Schematic indicating parameter (shear mobility, effective viscosity) extraction from step-edge film profiles. Calculated (c) shear mobility and (d) effective viscosity versus time at various distances from the free surface (FS) to the interior of the film.

stress, τ = 174 Pa at T_g + 52 °C. The step-edge profile was recorded at four different time intervals of t = 0, 10, 20, and 30 min. As expected, the shape of the step-edge profile changes due to the applied shear stress. Beyond this time dependence, the shape change exhibits a strong dependence on depth within the film, with large deformations near the free surface and negligible deformation near the substrate. As will be discussed below, these observations suggest the existence of regions of reduced and enhanced mobility at the substrate and free interfaces, respectively.

As shown in Figure 2b, we determined an effective local viscosity as a function of depth within the film via a procedure previously outlined by Scarpulla[40] and Mate[41] for molecular and polymeric liquids at room temperature. For each layer, we define a shear mobility $\chi_s(h)$ that represents how easily the molecules in a layer parallel to the free surface can be moved in the horizontal plane as

$$\chi_s(h) = \frac{\Delta x(h)}{\tau t} \quad (1)$$

where $\Delta x(h)$ is the lateral deformation at height h from substrate, τ is the applied shear stress, and t is the time elapsed since the start of shear. The effective viscosity is then computed from the layer-resolved shear mobility via the equation

DOI: 10.1021/acs.jpclett.7b00214
J. Phys. Chem. Lett. 2017, 8, 1229−1234

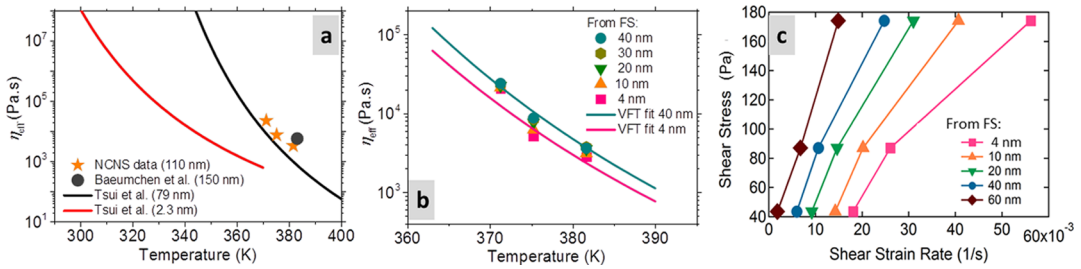

Figure 3. (a) Comparison of average effective viscosity data (stars) for low M_w (2.5 kDa) PS films in this work and in literature (M_w is the same or comparable). Solid lines correspond to VFT fit of data from Tsui et al.[30] at two film thicknesses. The higher film thickness (79 nm) also compares to bulk viscosity data. Circle is for capillary leveling data from Bäumchen et al.[33] (b) Local viscosity near free surface versus temperature. The representative data are obtained from NCNS testing of ∼110 nm PS film under 174 Pa at 108.5 °C for 30 min. Solid lines represent VFT fits of effective viscosities at two locations inside the film, 4 and 40 nm from free surface (FS). (c) Stress−strain rate relationship shows shear thinning in the vicinity of free surface. The data points are obtained from short-time (5 min) blow-off measurements applying different level of stress on ∼110 nm PS films at 108.5 °C.

$$\eta_{\mathrm{eff}}(h) = \left[\frac{\mathrm{d}\chi_s(h)}{\mathrm{d}h}\right]^{-1} \tag{2}$$

Hence, the NCNS approach provides a platform for the determination of spatially resolved viscoelastic functions, including viscosity.

As shown by Figure 2c, shear mobility in a 110 nm thick PS film is greatest near the free surface and is gradually reduced in the film interior. The layer-resolved effective viscosity, illustrated in Figure 2d, exhibits a corresponding gradient with a lower value at the free surface than in the film interior. Notably, the gradient of viscosity away from the free surface decreases and the shear mobility increases with increasing load time of the shear stress. Specifically, near the free surface, we find a slight decrease in η_{eff} with increasing shearing time. In contrast, there is a greater influence of shear time on the η_{eff} in the film interior. Hence, at t = 10 min, there is a factor of ∼3 difference in the near-surface viscosity and that of the film interior, while at t = 30 min, the near-surface viscosity is only slightly greater than that of the film interior. This quenching of the strength of the interfacial gradient under prolonged deformation is qualitatively similar to Riggleman et al.'s finding[42] that deformation tends to suppress spatial variations in mobility in a model-simulated bulk polymer glass. While that study focused on heterogeneities in a bulk sample[42] and the present work focuses on suppression of near-interface dynamic heterogeneity in a glass forming liquid (heterogeneity that has previously been observed in both experiments[15,16,23,30] and simulations[24−27]), these results contribute to an emerging picture, within which deformation tends to both enhance[43,44] and homogenize the dynamics of glasses and glass-forming liquids.

By applying the NCNS method at different temperatures, we probed the temperature dependence of η_{eff} both for the overall film and in a layer-resolved manner. As shown in Figure S3, tilting of the step-edge profile is reduced as temperature is decreased toward T_g in a 110 nm film. In Figure 3a, we compare the temperature-dependent layer-averaged η_{eff} obtained by the NCNS method to that reported by Tsui et al.[30] (via observation of the dynamics of surface capillary waves) and Bäumchen et al.[33] (via observation of self-similar flow profile in a step-edge interface) for PS thin films. A good agreement between these three approaches is observed, indicating that NCNS is an effective approach to probe the viscoelastic properties of thin polymer films.

We can now extend this analysis to the temperature dependence of layer-resolved dynamics. In Figure 3b, we illustrate η_{eff} versus T at different distances away from the free surface after ∼30 min of shear with τ = 174 Pa. The solid lines represent fits to the Vogel−Fulcher−Tammann (VFT) expression

$$\eta_{\mathrm{eff}}(T) = \eta_{\mathrm{eff}}(\infty)\exp\left(\frac{B}{T - T_0}\right) \tag{3}$$

for η_{eff} at 4 and 40 nm away from the free surface. In the VFT expression,[21,30] B is a constant, $\eta_{\mathrm{eff}}(\infty)$ is the high-temperature viscosity, and T_0 is the divergent temperature of the equilibrium dynamics. For the similar low-M_w bulk PS, B = 1620 K and T_0 = 288 K were reported.[30] Following the analysis of Tsui and coworkers in their treatment of PS thin-film viscosity,[30] we held B constant and equal to the bulk value. Then, we allowed $\eta_{\mathrm{eff}}(\infty)$ and T_0 to be adjusted. We found that the best fit at the free surface (4 nm inside from free surface) was obtained when T_0 was 276 K; that is, 12 K below the bulk value and at the deep interior (40 nm inside from free surface) it is 9 K below the bulk value. This result is qualitatively in agreement with the widely reported observations of reduction in T_g at the free surface of a polymer thin film.[15,16,23,30,38] Moreover, these results can be compared with those of Tsui and coworkers.[30] On the basis of an observed decrease in viscosity with decreasing film thickness, they inferred the existence of a reduced-viscosity layer at the free surface. Even more suggestively, a second study reported the presence of a highly mobile surface layer within a polymer film step edge, based again on a two-layer interpretation of mean deformation data. Our findings provide direct confirmation of this hypothesis, demonstrating that viscosity is reduced in a smooth gradient at the free surface, as is captured coarsely within a two-layer model.

In addition to providing depth resolution, the NCNS method also allows shear stress to be systematically varied. This permits a layer-resolved study of the shear thinning response of PS thin films. As shown in Figure 3c, this approach reveals that dynamics near the free surface are more susceptible to shear thinning than those within the film interior. This result, in general, supports prior observations of pronounced shear thinning on thin liquid polymer films upon confinement.[20,45]

To obtain further insight into the viscosity gradients revealed by the NCNS method, we performed molecular dynamics simulations of an NCNS experiment. We specifically studied

DOI: 10.1021/acs.jpclett.7b00214
J. Phys. Chem. Lett. 2017, 8, 1229−1234

NCNS on a model bead−spring polymer film[46,47] supported by a rigid crystalline substrate (shown in Figure S4), with segment/wall-bead interactions of strength equal to that of segment/segment interactions. A detailed simulation methodology is provided in the Supporting Information. In summary, the film spans periodic boundary conditions in the substrate plane; this geometry avoids the problem of being unable to reach the lubrication limit for the leading edge due to the limited length scales accessible to simulations. Simulations of the film NCNS process are performed at a reduced Lennard-Jones (LJ) temperature of $T = 0.5$, within the glass-formation range of this polymer. The surface-stress imposed on the film during experimental NCNS is modeled by continuously subjecting all polymer segments at a distance $>20\sigma$ from the substrate to a force of 0.01 (where both distance and force are in dimensionless LJ units) in the positive x direction. This corresponds to application of the surface force to ∼1.5 monomer layers, physically consistent with the transfer of gas momentum into the fluid by surface collisions with nitrogen molecules during the experimental NCNS.

A film velocity gradient is extracted from these simulations based on a layer-resolved steady-state displacement rate (see the Supporting Information). As shown in Figure 4a, the imposed surface shear stress leads to a steady-state velocity gradient that is qualitatively consistent with experimental displacement profiles: It is nonlinear, with a larger gradient near the free surface and a smaller gradient near the substrate. Applying the steady-state equations of 1D shear flow as in the experimental data analysis then yields viscosity profiles at each temperature shown in Figure 4b. As in the experimental results, the shear viscosity is suppressed near the free surface and enhanced near the substrate.

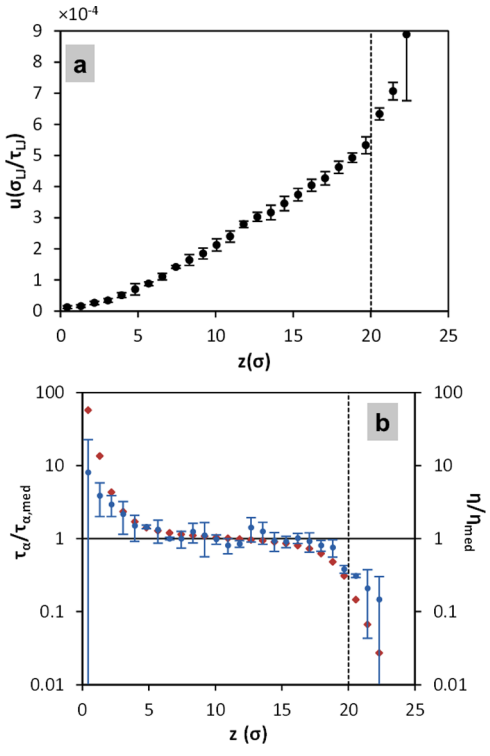

Figure 4. Simulated: (a) Mean velocity, u, versus distance z from the substrate. (b) Inferred viscosity (blue circles) from blowing simulations and mean segmental relaxation time (red diamonds) from quiescent simulations, each normalized by their median value across all bins as a function of distance z from the substrate. The vertical dashed line is the lower bound of stress application in the blow-off simulation. Error bars are standard deviations from four independent runs.

What could be the origin of the viscosity gradient observed in experiments and simulations? First, we test whether this could emerge from a gradient in chain orientation by quantifying gradients in the orientational correlation function describing the tendency of chain end-to-end vectors to orient parallel to the direction to the film surfaces. As shown in Figure S5, this quantity exhibits a short-ranged negative peak near both surfaces, indicating that chains tend to be oriented in plane very near to both the substrate and free surface. Given the short range of this gradient and its nearly symmetric nature, this cannot explain the viscosity gradients observed in these simulations and experiments.

Next, we ask whether these viscosity gradients reflect gradients in segmental relaxation time and T_g that have been previously quantified in simulations[25,27] and experiments.[15,17] We perform an additional set of simulations in which we collect relaxation data for the quiescent film. We then compute a quiescent mean segmental relaxation time τ_α for particles in bins as a function of distance from the substrate, as in the determination of the velocity profile. As shown in Figure 4b, the resulting gradient in τ_α is similar to the gradient in inferred viscosity, albeit with greater shifts near the film interfaces. This can be understood by considering the fact that viscosity probes the chain's lowest Rouse mode dynamics, whereas segmental dynamics probe the chain's highest Rouse mode dynamics. The former can be expected to average over the local segmental dynamics over a length scale related to the chain's mean end-to-end distance, naturally yielding an attenuation of the gradient in segmental-scale dynamics. Thus, our simulation results indicate a direct correlation between gradients in molecular mobility (viscosity) and the average segmental relaxation time.

The dynamics, mechanics, and viscous relaxation behavior of polymers in films and in the nanoscale vicinity of interfaces remains one of the enduring scientific and technological challenges of the modern push toward nanostructured materials. Here we demonstrate that a NCNS method provides nanoscale resolution of depth-dependent mobility and viscosity gradients in thin polymer films. Simulations indicate that these gradients in viscosity for these low-molecular-weight chains directly reflect an underlying gradient in segmental dynamics, associated with the previously reported suppressions in glass-transition temperature near free surfaces. Moreover, these gradients tend to weaken with increasingly long shear times, consistent with an emerging picture wherein deformation tends to suppress dynamical heterogeneities in glasses and glass-forming liquids. Looking forward, NCNS has the potential to open the door to a new era of depth-resolved dynamical measurements in thin polymer films.

EXPERIMENTAL METHODS

Thin films of PS (M_w = 2.5 kDa, with PDI of 1.06, $T_{g,bulk}$= 56.8 °C) were prepared by spin-coating atop Si/SiO_x substrates. Subsequently, a portion of the film was removed from the substrate via mechanical cleavage to create a sharp step-edge. Before each experiment, the step-edge profile of each film was recorded via atomic force microscopy (AFM, Veeco Dimension V Nanoman). To initiate the experiment, the films were loaded into the flow cell such that the direction of the applied shear stress was perpendicular to the step-edge and then subjected to

DOI: 10.1021/acs.jpclett.7b00214
J. Phys. Chem. Lett. 2017, 8, 1229−1234

nanoshear at a temperature above the T_g. The evolution of the step-edge profile was monitored intermittently via AFM. Dewetting and thermal annealing experiments were done in situ on AFM heating stage (Asylum Research MFP-3D-SA) acquiring images at regular intervals to track temporal changes of the step-edge held at a fixed temperature. Typically, areas of $10 \times 50\ \mu m^2$ in the topography images were analyzed to obtain the data of the film profile. Furthermore, we made sure that at each time approximately the same area was scanned under AFM to track temporal changes. See the Supporting Information for further details on the film fabrication process and the AFM data analysis protocol.

■ ASSOCIATED CONTENT

Supporting Information

The Supporting Information is available free of charge on the ACS Publications website at DOI: 10.1021/acs.jpclett.7b00214.

Control experiments to ensure role of shearing during NCNS, optical microscopy, temperature dependence of NCNS, film fabrication method, NCNS flow-cell apparatus and setup, AFM data analysis, MD simulation methodology, and Figures S1−S5. (PDF)

■ AUTHOR INFORMATION

Corresponding Authors

*E-mail: dsimmons@uakron.edu (D.S.S.)
*E-mail: rpriestl@princeton.edu (R.D.P.).

ORCID

Mithun Chowdhury: 0000-0002-2513-6006
David S. Simmons: 0000-0002-1436-9269
Rodney D. Priestley: 0000-0001-6765-2933

Author Contributions

⊥M.C. and Y.G. made equal contributions.

Notes

The authors declare no competing financial interest.

■ ACKNOWLEDGMENTS

R.D.P., M.C., and Y.W. acknowledge support of the National Science Foundation (NSF) Materials Research Science and Engineering Center program through the Princeton Center for Complex Materials (DMR-1420541). D.S.S., W.L.M., and J.H.M. acknowledge support from National Science Foundation Grant DMR-1310433. This work used the Extreme Science and Engineering Discovery Environment (XSEDE), which is supported by National Science Grant OCI-1053575. Helpful discussion with Günter Reiter is gratefully acknowledged.

■ REFERENCES

(1) Keten, S.; Xu, Z.; Ihle, B.; Buehler, M. J. Nanoconfinement Controls Stiffness, Strength and Mechanical Toughness of [beta]-sheet Crystals in Silk. *Nat. Mater.* **2010**, *9*, 359−367.

(2) Guo, Y.; Morozov, A.; Schneider, D.; Chung, J. W.; Zhang, C.; Waldmann, M.; Yao, N.; Fytas, G.; Arnold, C. B.; Priestley, R. D. Ultrastable Nanostructured Polymer Glasses. *Nat. Mater.* **2012**, *11*, 337−343.

(3) Bhandaru, N.; Das, A.; Mukherjee, R. Confinement Induced Ordering in Dewetting of Ultra-Thin Polymer Bilayers on Nano-patterned Substrates. *Nanoscale* **2016**, *8*, 1073−1087.

(4) Napolitano, S. Staying Conductive in the Stretch. *Science* **2017**, *355*, 24−25.

(5) Ouyang, J.; Chu, C.-W.; Szmanda, C. R.; Ma, L.; Yang, Y. Programmable Polymer Thin Film and Non-volatile Memory Device. *Nat. Mater.* **2004**, *3*, 918−922.

(6) Napolitano, S.; Glynos, E.; Tito, N. B. Glass Transition of Polymers in Bulk, Confined Geometries, and Near Interfaces. *Rep. Prog. Phys.* **2017**, *80*, 036602.

(7) Nygård, K.; Satapathy, D.; Buitenhuis, J.; Perret, E.; Bunk, O.; David, C.; Van Der Veen, J. Confinement-induced Orientational Alignment of Quasi-2D Fluids. *Eur. Phys. Lett.* **2009**, *86*, 66001.

(8) Chandran, S.; Begam, N.; Padmanabhan, V.; Basu, J. Confinement Enhances Dispersion in Nanoparticle–Polymer Blend Films. *Nat. Commun.* **2014**, *5*, 3697.

(9) Alcoutlabi, M.; McKenna, G. B. Effects of Confinement on Material Behaviour at the Nanometer Size Scale. *J. Phys.: Condens. Matter* **2005**, *17*, R461−R524.

(10) Isaacson, S. G.; Lionti, K.; Volksen, W.; Magbitang, T. P.; Matsuda, Y.; Dauskardt, R. H.; Dubois, G. Fundamental Limits of Material Toughening in Molecularly Confined Polymers. *Nat. Mater.* **2015**, *15*, 294−298.

(11) Tweedie, C. A.; Constantinides, G.; Lehman, K. E.; Brill, D. J.; Blackman, G. S.; Van Vliet, K. J. Enhanced Stiffness of Amorphous Polymer Surfaces under Confinement of Localized Contact Loads. *Adv. Mater.* **2007**, *19*, 2540−2546.

(12) Rowland, H. D.; King, W. P.; Pethica, J. B.; Cross, G. L. Molecular Confinement Accelerates Deformation of Entangled Polymers During Squeeze Flow. *Science* **2008**, *322*, 720−724.

(13) Geng, K.; Katsumata, R.; Yu, X.; Ha, H.; Dulaney, A. R.; Ellison, C. J.; Tsui, O. K. C. Conflicting Confinement Effects on the T_g, Diffusivity, and Effective Viscosity of Polymer Films: A Case Study with Poly(isobutyl methacrylate) on Silica and Possible Resolution. *Macromolecules* **2017**, *50*, 609−617.

(14) Starr, F. W.; Douglas, J. F.; Meng, D.; Kumar, S. K. Bound Layers "Cloak" Nanoparticles in Strongly Interacting Polymer Nanocomposites. *ACS Nano* **2016**, *10*, 10960−10965.

(15) Ellison, C. J.; Torkelson, J. M. The Distribution of Glass-Transition Temperatures in Nanoscopically Confined Glass Formers. *Nat. Mater.* **2003**, *2*, 695−700.

(16) Jones, R. A. Amorphous Materials: Glasses with Liquid-like Surfaces. *Nat. Mater.* **2003**, *2*, 645−646.

(17) Priestley, R. D.; Ellison, C. J.; Broadbelt, L. J.; Torkelson, J. M. Structural Relaxation of Polymer Glasses at Surfaces, Interfaces, and in Between. *Science* **2005**, *309*, 456−459.

(18) Oh, H.; Green, P. F. Polymer Chain Dynamics and Glass Transition in Athermal Polymer/Nanoparticle Mixtures. *Nat. Mater.* **2009**, *8*, 139−143.

(19) Chowdhury, M.; Freyberg, P.; Ziebert, F.; Yang, A. C.-M.; Steiner, U.; Reiter, G. Segmental Relaxations have Macroscopic Consequences in Glassy Polymer Films. *Phys. Rev. Lett.* **2012**, *109*, 136102.

(20) Chandran, S.; Reiter, G. Transient Cooperative Processes in Dewetting Polymer Melts. *Phys. Rev. Lett.* **2016**, *116*, 088301.

(21) Chowdhury, M.; Al Akhrass, S.; Ziebert, F.; Reiter, G. Relaxing Nonequilibrated Polymers in Thin Films at Temperatures Slightly Above the Glass Transition. *J. Polym. Sci., Part B: Polym. Phys.* **2017**, *55*, 515−523.

(22) Burroughs, M. J.; Napolitano, S.; Cangialosi, D.; Priestley, R. D. Direct Measurement of Glass Transition Temperature in Exposed and Buried Adsorbed Polymer Nanolayers. *Macromolecules* **2016**, *49*, 4647−4655.

(23) Priestley, R. D.; Cangialosi, D.; Napolitano, S. On the Equivalence Between the Thermodynamic and Dynamic Measurements of the Glass Transition in Confined Polymers. *J. Non-Cryst. Solids* **2015**, *407*, 288−295.

(24) Baschnagel, J.; Varnik, F. Computer Simulations of Supercooled Polymer Melts in the Bulk and in Confined Geometry. *J. Phys.: Condens. Matter* **2005**, *17*, R851−R953.

(25) Lang, R. J.; Merling, W. L.; Simmons, D. S. Combined Dependence of Nanoconfined T_g on Interfacial Energy and Softness of Confinement. *ACS Macro Lett.* **2014**, *3*, 758−762.

DOI: 10.1021/acs.jpclett.7b00214
J. Phys. Chem. Lett. 2017, 8, 1229−1234

(26) Simmons, D. S. An Emerging Unified View of Dynamic Interphases in Polymers. *Macromol. Chem. Phys.* **2016**, *217*, 137−148.
(27) Hanakata, P. Z.; Douglas, J. F.; Starr, F. W. Interfacial Mobility Scale Determines the Scale of Collective Motion and Relaxation Rate in Polymer Films. *Nat. Commun.* **2014**, *5*, 4163.
(28) Gao, S.; Koh, Y. P.; Simon, S. L. Calorimetric Glass Transition of Single Polystyrene Ultrathin Films. *Macromolecules* **2013**, *46*, 562−570.
(29) McGraw, J. D.; Salez, T.; Bäumchen, O.; Raphaël, E.; Dalnoki-Veress, K. Self-Similarity and Energy Dissipation in Stepped Polymer Films. *Phys. Rev. Lett.* **2012**, *109*, 128303.
(30) Yang, Z.; Fujii, Y.; Lee, F. K.; Lam, C.-H.; Tsui, O. K. Glass Transition Dynamics and Surface Layer Mobility in Unentangled Polystyrene Films. *Science* **2010**, *328*, 1676−1679.
(31) Guo, Y.; Zhang, C.; Priestley, R. D. Polymer Thin Film Instability from a Patterned Edge. *Appl. Phys. Lett.* **2014**, *105*, 041603.
(32) Chen, F.; Peng, D.; Lam, C.-H.; Tsui, O. K. Viscosity and Surface-Promoted Slippage of Thin Polymer Films Supported by a Solid Substrate. *Macromolecules* **2015**, *48*, 5034−5039.
(33) Rivetti, M.; Salez, T.; Benzaquen, M.; Raphaël, E.; Bäumchen, O. Universal Contact-Line Dynamics at the Nanoscale. *Soft Matter* **2015**, *11*, 9247−9253.
(34) Liu, Y.; Chen, Y.-C.; Hutchens, S.; Lawrence, J.; Emrick, T.; Crosby, A. J. Directly Measuring the Complete Stress–Strain Response of Ultrathin Polymer Films. *Macromolecules* **2015**, *48*, 6534−6540.
(35) Stafford, C. M.; Harrison, C.; Beers, K. L.; Karim, A.; Amis, E. J.; VanLandingham, M. R.; Kim, H.-C.; Volksen, W.; Miller, R. D.; Simonyi, E. E. A Buckling-based Metrology for Measuring the Elastic Moduli of Polymeric Thin Films. *Nat. Mater.* **2004**, *3*, 545−550.
(36) O'Connell, P.; McKenna, G. Rheological Measurements of The Thermoviscoelastic Response of Ultrathin Polymer Films. *Science* **2005**, *307*, 1760−1763.
(37) Fakhraai, Z.; Forrest, J. Measuring the Surface Dynamics of Glassy Polymers. *Science* **2008**, *319*, 600−604.
(38) Chai, Y.; Salez, T.; McGraw, J. D.; Benzaquen, M.; Dalnoki-Veress, K.; Raphaël, E.; Forrest, J. A. A Direct Quantitative Measure of Surface Mobility in a Glassy Polymer. *Science* **2014**, *343*, 994−999.
(39) Derjaguin, B.; Karassev, V. Viscosity Studies of Liquid Boundary Layers by the Blow-Off Method. *Prog. Surf. Sci.* **1992**, *40*, 301−308.
(40) Scarpulla, M. A.; Mate, C. M.; Carter, M. D. Air Shear Driven Flow of Thin Perfluoropolyether Polymer Films. *J. Chem. Phys.* **2003**, *118*, 3368−3375.
(41) Mate, C. M.; Marchon, B. Shear Response of Molecularly Thin Liquid Films to an Applied Air Stress. *Phys. Rev. Lett.* **2000**, *85*, 3902.
(42) Riggleman, R. A.; Lee, H.-N.; Ediger, M.; De Pablo, J. J. Heterogeneous Dynamics during Deformation of a Polymer Glass. *Soft Matter* **2010**, *6*, 287−291.
(43) Lee, H.-N.; Paeng, K.; Swallen, S. F.; Ediger, M. Direct Measurement of Molecular Mobility in Actively Deformed Polymer Glasses. *Science* **2009**, *323*, 231−234.
(44) Roth, C. B. Mobility and Stability of Glasses. *J. Polym. Sci., Part B: Polym. Phys.* **2010**, *48*, 2558−2560.
(45) Yamada, S. General Shear-Thinning Dynamics of Confined Fluids. *Tribol. Lett.* **2002**, *13*, 167−171.
(46) Kremer, K.; Grest, G. S. Dynamics of Entangled Linear Polymer Melts: A Molecular-Dynamics Simulation. *J. Chem. Phys.* **1990**, *92*, 5057−5086.
(47) Mackura, M. E.; Simmons, D. S. Enhancing Heterogenous Crystallization Resistance in a Bead-Spring Polymer Model by Modifying Bond Length. *J. Polym. Sci., Part B: Polym. Phys.* **2014**, *52*, 134−140.

DOI: 10.1021/acs.jpclett.7b00214
J. Phys. Chem. Lett. 2017, 8, 1229−1234